

Supporting Information

Insights into the durability of Co-Fe spinel oxygen evolution electrocatalysts via *operando* studies of catalyst structure

Laura Calvillo^{1,*}, Francesco Carraro¹, Olena Vozniuk², Verónica Celorrio^{3,Φ}, Luca Nodari⁴,
Andrea E. Russell⁵, Doriana Debellis,⁶ David Fermin³, Fabrizio Cavani², Stefano Agnoli¹,
Gaetano Granozzi¹

¹ Dipartimento di Scienze Chimiche, Università di Padova and INSTM Research Unit, Via
Marzolo 1, 35131 Padova, Italia

² Dipartimento di Chimica Industriale “Toso Montanari”, Università di Bologna, Viale
Risorgimento 4, 40136 Bologna, Italia

³ School of Chemistry, University of Bristol, Cantocks Close, BS8 1TS, Bristol, UK

⁴ Istituto per l’Energetica e le Interfasi CNR-IENI and INSTM, Corso Stati Uniti, 4, 35127
Padova, Italia

⁵ Chemistry, University of Southampton, Highfield, Southampton SO17 1BJ, UK

⁶ Istituto Italiano di Tecnologia, Via Morego 30, 16163 Genova, Italia

*Corresponding author: laura.calvillolamana@unipd.it

ΦCurrent Address:

UK Catalysis Hub, Research Complex at Harwell, RAL, Oxford, OX11 0FA, UK. And
Kathleen Lonsdale Building, Department of Chemistry, University College London, Gordon
Street, London, WC1H 0AJ, UK.

Description of the UHV system

The system consists of two independent UHV chambers: a preparation/analysis chamber and an electrochemical (EC) chamber. In the former, the sample is prepared using the procedure described below and characterised by XPS. The EC chamber is coupled to the preparation chamber by means of a UHV-EC transfer system. This consists of two manipulators (horizontal and vertical) and is attached to the main preparation chamber through a gate valve. The horizontal manipulator is used to transfer the sample from the preparation to the EC chamber, whereas the vertical one allows the coupling of the sample to the EC cell, which is connected to the EC chamber from the top.

Preparation and characterization of the Co-Fe oxide films on Pd(100)

First, the surface of the Pd(100) single crystal (MaTeck), was cleaned by repeated cycles of sputtering (2 keV Argon ions at 300 K) and annealing (at 900 K). The residual carbon was removed by annealing in 2.0×10^{-5} Pa of oxygen at 700 K and, subsequently, the adsorbed oxygen was removed by flash at 900 K. The Co-Fe oxide films were deposited by consecutive reactive evaporation of Co and/or Fe (0.35 ML min^{-1}) onto clean Pd(100) substrate in 1×10^{-4} Pa O_2 partial pressure at room temperature (RT). Then, the samples were annealed in oxygen atmosphere at 673 K for 60 min in $P(\text{O}_2) = 1 \times 10^{-3}$ Pa in order to favour the formation of the mixed Co-Fe spinel structure. The thickness of the films was 2-3 nm.

The chemical composition of the samples and the chemical changes induced by the exposure to the EC environment were investigated by XPS using an EA 125 Omicron electron analyzer equipped with five channeltrons, working at a base pressure of 10^{-8} Pa. The XPS data were collected at RT with the Al $K\alpha$ line ($h\nu = 1486.6 \text{ eV}$) of a non-monochromatized dual-anode DAR400 X-ray source using 0.1 eV energy steps, 0.5 s collection time, and 20 eV pass energy. The binding energy (BE) scale was calibrated using a gold sample (Au 4f at 84 eV).

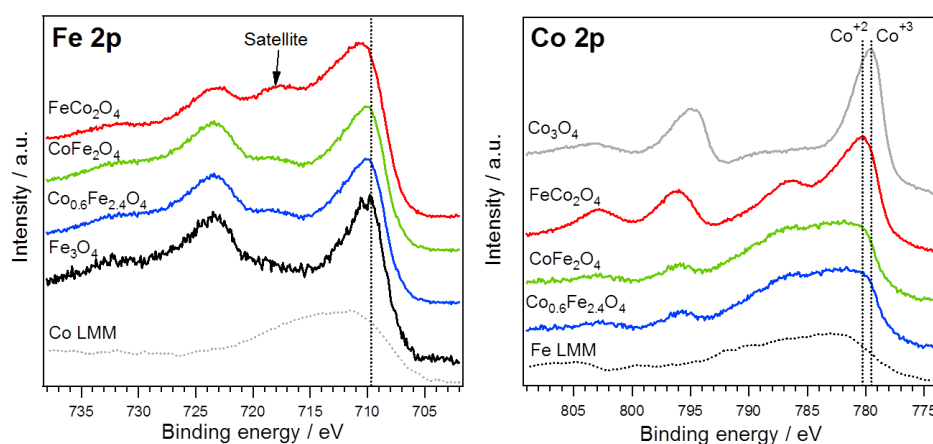


Figure S1. High-resolution Fe 2p and Co 2p photoemission spectra of the as-prepared Co-Fe oxide films on Pd(100) substrate. The monometallic Fe₃O₄ and Co₃O₄ films were also prepared as reference.

Figure S1 shows the Fe 2p and Co 2p photoemission lines for the as-prepared Co-Fe oxide films with different composition. The presence of the Co LMM and Fe LMM lines overlapping the Fe 2p and Co 2p regions complicates the interpretation of the results. The analysis of the Co 2p and Fe 2p lines for the monometallic oxides confirm the formation of the Co_3O_4 and Fe_3O_4 phases with spinel structure.¹ The presence of a satellite peak at 719.3 eV in the Fe 2p photoemission lines of the Co-Fe mixed oxides indicates that the oxidation state of Fe is +3, as expected. It should be notice that the presence of the Co LMM line overlapping the Fe 2p region results in a no-real shift of the Fe $2p_{3/2}$ peak toward higher binding energies (BEs), which becomes more significant as the amount of Co increases.

The analysis of the Co 2p region indicates that the FeCo_2O_4 film contains Co(II) and Co(III) species, and the spectrum is comparable to the one obtained for the corresponding sample in form of powder (Figure S2). In the case of the two films with lower amount of Co, the strong contribution of the Fe LMM line makes difficult the determination of the oxidation state of Co. However, the shoulder at around 787 eV suggests the presence of Co(II) species.

Synthesis of Co-Fe spinel powders.

Cobalt ferrosinels with different Co:Fe atomic ratio (1:2 and 0.6:2.4) were prepared by the co-precipitation method previously described in [2]. Briefly, 150 mL of a solution containing the Co and Fe precursors ($\text{Co}(\text{NO}_3)_2 \cdot \text{H}_2\text{O}$ and $\text{Fe}(\text{NO}_3)_3 \cdot 9\text{H}_2\text{O}$, Sigma-Aldrich) were added drop by drop to 500 mL of 2 M NaOH solution at 50 °C under vigorous stirring, and kept at this temperature under stirring for 2 h. During this time, 3 M NaOH was added in order to keep the pH above 13. Subsequently, the suspension was filtered and washed with 1.5 L of distilled water at room temperature. Finally, the powders were dried in air at 120 °C for 12 h and then calcined at 450 °C for 8 h. For the synthesis of the iron cobaltite (atomic Fe:Co ratio of 1:2), appropriate amounts of FeCl_3 and $\text{CoCl}_2 \cdot 6\text{H}_2\text{O}$ were dissolved in distilled water and added to a boiling 2M KOH solution under vigorous stirring. Then, the solution was stirred at the same temperature for 2 h, maintaining the pH above 12. Subsequently, the suspension was filtered and washed with boiling water. The powders were dried in air at 200 °C and finally annealed at 400° C for 1.5 h and at 900 °C for 6 h.

Structural and morphological characterization of the fresh Co-Fe oxide powders.

XRD, XPS and TEM.

X-Ray diffraction (XRD) was performed with a Bruker D8 Advance diffractometer, configured with a Bragg-Brentano geometry and equipped with a Bruker Lynx Eye detector, operating with Cu K_α radiation ($\lambda = 0.15406$ nm). Transmission electron microscopy (TEM) images were obtained using a JEOL JEM-1400Plus. X-ray photoelectron spectroscopy (XPS) data was obtained in a custom designed UHV system equipped with an EA 125 Omicron electron analyzer with five channeltrons, working at a base pressure of 10^{-10} mbar. Core level photoemission spectra (C 1s, O 1s, Co 2p and Fe 2p regions) were collected in normal

emission at room temperature with a non-monochromatized Mg K_{α} X-ray source (1253.6 eV).

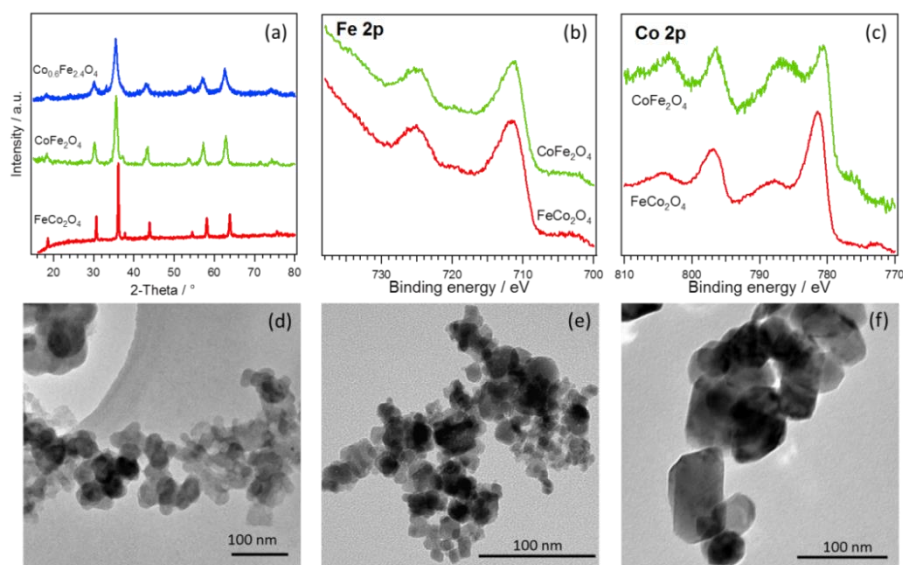


Figure S2. XRD patterns (a); Fe 2p (b) and Co 2p (c) XPS regions; and TEM images (d-f) of the $\text{Co}_{0.6}\text{Fe}_{2.4}\text{O}_4$ (d), CoFe_2O_4 (e), and FeCo_2O_4 (f) samples.

Ex situ XAS.

X-ray adsorption measurements were recorded on beamline B18 at Diamond Light Source (UK) with ring energy of 3 GeV and a current of 300 mA. The monochromator used was Si(311) crystals operating in Quick EXAFS (QEXAFS) mode. Pellets of the different spinels were measured in transmission mode at the Co K (7709 eV) and Fe K (7112 eV) absorption edges at 298 K using a 36-element Ge detector. The corresponding foils were measured simultaneously. Calibration of the monochromator was carried out using the Co and Fe foils previously to the measurements. The acquired data was processed and analyzed using the Athena and Artemis programs,³ respectively, which implement the FEFF6 and IFEFFIT codes.⁴ Fits were carried out using a k range of 2.75 – 10 \AA^{-1} and 2.75 – 13 \AA^{-1} for the Fe K and Co K edge, respectively, and an R range of 1.0 – 3.8 \AA with multiple k weightings of 1, 2 and 3.

Table S1. Cation distribution in the Fe-Co spinels determined from Mössbauer spectroscopy and EXAFS. The Th and Oh subscripts indicate the tetrahedral and octahedral positions.

Sample	Mössbauer	EXAFS	$\frac{\text{Co}_{\text{Oh}}}{\text{Co}_{\text{Td}}}$	$\frac{\text{Fe}_{\text{Oh}}}{\text{Fe}_{\text{Td}}}$
$\text{Co}_{0.6}\text{Fe}_{2.4}\text{O}_4$	---	$(\text{Co}_{0.16}\text{Fe}_{0.84})_{\text{Td}}(\text{Co}_{0.44}\text{Fe}_{1.56})_{\text{Oh}}$	2.7	1.8
CoFe_2O_4	$(\text{Co}_{0.26}\text{Fe}_{0.74})_{\text{Td}}(\text{Co}_{0.74}\text{Fe}_{1.26})_{\text{Oh}}$	$(\text{Co}_{0.30}\text{Fe}_{0.70})_{\text{Td}}(\text{Co}_{0.70}\text{Fe}_{1.30})_{\text{Oh}}$	2.3	1.8
FeCo_2O_4	$(\text{Co}_{0.56}\text{Fe}_{0.44})_{\text{Td}}(\text{Co}_{1.44}\text{Fe}_{0.56})_{\text{Oh}}$	$(\text{Co}_{0.62}\text{Fe}_{0.38})_{\text{Td}}(\text{Co}_{1.38}\text{Fe}_{0.62})_{\text{Oh}}$	2.2	1.6

Figure S3 shows the *ex situ* XANES spectra for the three Co-Fe spinels and the oxides used as reference to establish the linear correlation between the K-edge excitation energy and the metal oxidation state.^{5,6,7} For the three samples, the edge position at the Fe K edge indicates that the oxidation state of Fe is close to +3 as expected (Figure S3c). In the case of the $\text{Co}_{0.6}\text{Fe}_{2.4}\text{O}_4$ sample, the global oxidation state is slightly lower due to the presence of Fe^{2+} to compensate the lower amount of Co ($\text{Co}_{0.6}^{2+}\text{Fe}_{0.4}^{2+}\text{Fe}_{2.3}^{3+}\text{O}_4$). At the Co K-edge, slight differences are observed for the three samples. The oxidation state of Co is close to +2 in $\text{Co}_{0.6}\text{Fe}_{2.4}\text{O}_4$ as expected, whereas in CoFe_2O_4 is close to +2.2. In FeCo_2O_4 , however, the oxidation state of Co is around 2.5, confirming the presence of both Co^{2+} and Co^{3+} ($\text{Co}^{2+}\text{Fe}^{3+}\text{Co}^{3+}\text{O}_4$).

From the analysis of the EXAFS region, the cation distribution was determined (Table S1). The parameters extracted from the EXAFS fits are reported in Tables S3-S4, whilst the Fourier transformed EXAFS spectra and the corresponding k-space spectra are depicted in Figure S4. In order to confirm the quality of the fits, the cation distribution was also studied by Mössbauer spectroscopy (Figure 4). Table S1 summarizes the results obtained by the two techniques, which are in good agreement.

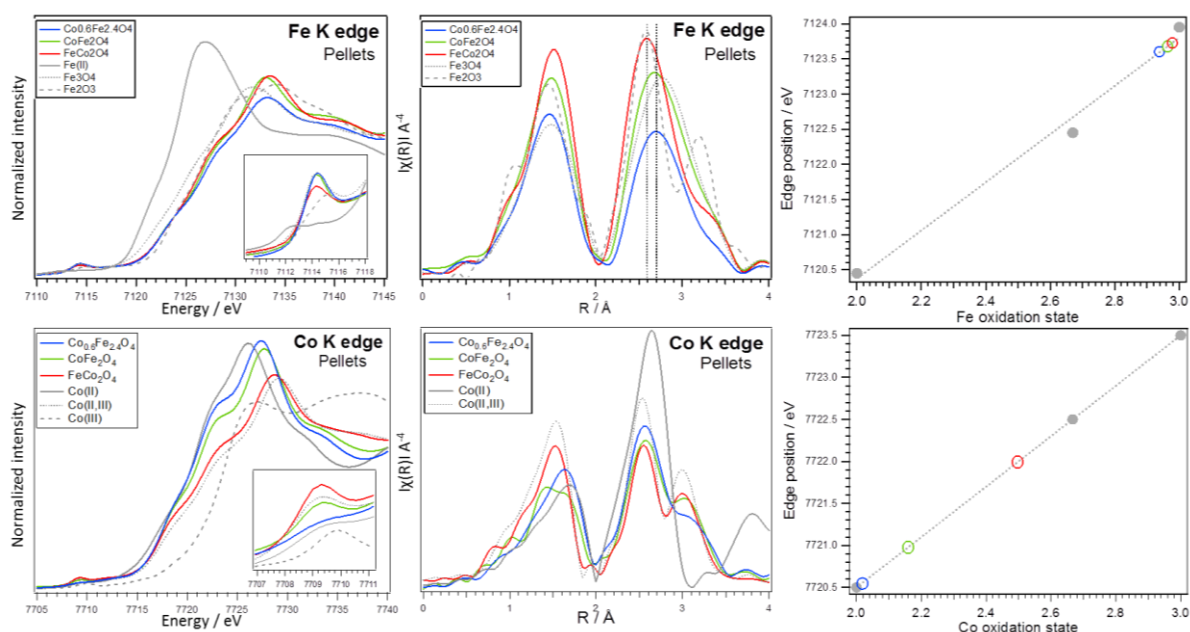


Figure S3. XANES spectra (left panels), Fourier transformed EXAFS spectra (middle panels), and oxidation state (right panels) at Fe K (upper panels) and Co K (bottom panels) edges for the FeCo_2O_4 (red), CoFe_2O_4 (green) and $\text{Co}_{0.6}\text{Fe}_{2.4}\text{O}_4$ (blue) spinels. The inset in the left panels corresponds to the zoom of the pre-edge peak.

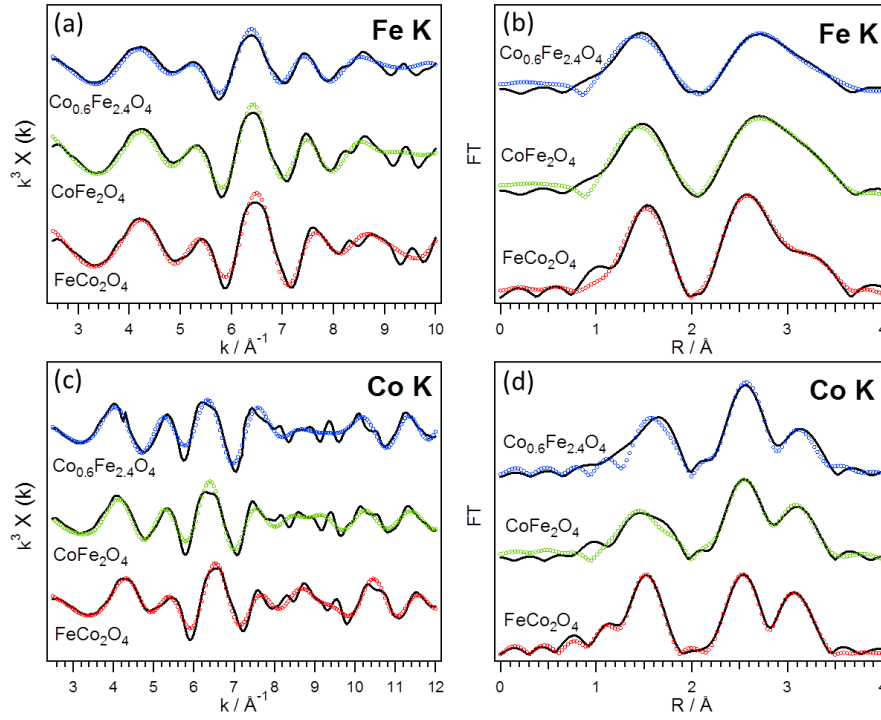


Figure S4. k^3 weighted experimental data (black) and fit (blue, green, red) (a,c) with the corresponding Fourier transform (b,d) for the Co-Fe spinels recorded at the Fe K (a,b) and Co K (c,d) edges.

Table S2. Structural parameters obtained for the $\text{Co}_{0.6}\text{Fe}_{2.4}\text{O}_4$ spinel from fitting simultaneously the Co K and Fe K edge EXAFS data acquired under air. ($R_f = 0.011$)

Fe K edge ($E_0 = 3.69$)				Co K edge ($E_0 = -0.21$)			
Shell	N	R/Å	$\sigma^2 \times 10^4/\text{Å}^2$	Shell	N	R/Å	$\sigma^2 \times 10^4/\text{Å}^2$
$x_B = 0.65$				$x_B = 0.73$			
Fe _{Oh} -O	6	1.950 ± 0.044	172 ± 88	Co _{Oh} -O	6	2.066 ± 0.063	34 ± 13
Fe _{Oh} -M _{Oh}	6	3.008 ± 0.013	302 ± 178	Co _{Oh} -M _{Oh}	6	2.904 ± 0.053	65 ± 18
Fe _{Oh} -M _{Td}	6	3.481 ± 0.066	84 ± 50	Co _{Oh} -M _{Td}	6	3.481 ± 0.066	84 ± 50
$x_A = 0.35$				$x_A = 0.27$			
Fe _{Th} -O	4	1.585 ± 0.093	228 ± 44	Co _{Td} -O	4	1.932 ± 0.048	76 ± 53
Fe _{Td} -M _{Oh}	12	3.481 ± 0.066	84 ± 50	Co _{Td} -M _{Oh}	12	3.481 ± 0.066	84 ± 50
Fe _{Td} -M _{Td}	4	3.699 ± 0.087	58 ± 31	Co _{Td} -M _{Td}	4	3.528 ± 0.091	64 ± 44

Table S3. Structural parameters obtained for the CoFe_2O_4 spinel from fitting simultaneously the Co K and Fe K edge EXAFS data acquired under air. ($R_f = 0.011$)

Fe K edge ($E_0 = -1.47$)				Co K edge ($E_0 = -2.10$)			
Shell	N	R/Å	$\sigma^2 \times 10^4/\text{Å}^2$	Shell	N	R/Å	$\sigma^2 \times 10^4/\text{Å}^2$
$x_B = 0.65$				$x_B = 0.70$			
Fe _{Oh} -O	6	1.923 ± 0.024	273 ± 33	Co _{Oh} -O	6	1.968 ± 0.023	283 ± 50
Fe _{Oh} -M _{Oh}	6	3.014 ± 0.021	256 ± 25	Co _{Oh} -M _{Oh}	6	2.972 ± 0.017	203 ± 20
Fe _{Oh} -M _{Td}	6	3.436 ± 0.031	352 ± 29	Co _{Oh} -M _{Td}	6	3.436 ± 0.031	352 ± 29
$x_A = 0.35$				$x_A = 0.30$			
Fe _{Td} -O	4	1.560 ± 0.024	192 ± 47	Co _{Td} -O	4	1.593 ± 0.037	170 ± 61
Fe _{Td} -M _{Oh}	12	3.436 ± 0.031	352 ± 29	Co _{Td} -M _{Oh}	12	3.436 ± 0.031	352 ± 29
Fe _{Td} -M _{Td}	4	3.840 ± 0.045	142 ± 55	Co _{Td} -M _{Td}	4	3.824 ± 0.045	116 ± 57

Table S4. Structural parameters obtained for the FeCo_2O_4 spinel from fitting simultaneously the Co K and Fe K edge EXAFS data acquired under air. ($R_f = 0.006$)

Fe K edge ($E_0 = 2.69$)				Co K edge ($E_0 = 2.39$)			
Shell	N	R/Å	$\sigma^2 \times 10^4/\text{Å}^2$	Shell	N	R/Å	$\sigma^2 \times 10^4/\text{Å}^2$
$x_B = 0.62$				$x_B = 0.69$			
Fe _{Oh} -O	6	1.977 ± 0.014	118 ± 19	Co _{Oh} -O	6	1.943 ± 0.023	109 ± 28
Fe _{Oh} -M _{Oh}	6	2.960 ± 0.015	121 ± 14	Co _{Oh} -M _{Oh}	6	2.900 ± 0.017	46 ± 13
Fe _{Oh} -M _{Td}	6	3.470 ± 0.039	211 ± 37	Co _{Oh} -M _{Td}	6	3.470 ± 0.039	211 ± 37
$x_A = 0.38$				$x_A = 0.31$			
Fe _{Td} -O	4	1.636 ± 0.040	192 ± 47	Co _{Td} -O	4	1.593 ± 0.013	170 ± 61
Fe _{Td} -M _{Oh}	12	3.470 ± 0.039	211 ± 37	Co _{Td} -M _{Oh}	12	3.470 ± 0.039	211 ± 37
Fe _{Td} -M _{Td}	4	3.783 ± 0.045	235 ± 62	Co _{Td} -M _{Td}	4	3.824 ± 0.017	92 ± 23

Electrochemical characterization

In situ electrochemical characterization of films. The procedure is detailed in the main text.

Ex situ electrochemical characterization of powders. Electrochemical measurements were conducted in a three-electrode cell using a rotating disk electrode (RDE) fitted to an ALS

rotation controller and connected to CompactStat bipotentiostat (Ivium). The RDE electrode consisted of 4 mm glassy carbon disk. A mercury/mercurous oxide (Hg/HgO, calibrated as +0.918 V vs RHE) electrode (in 1M NaOH, IJ Cambria) was used as reference electrode and a Pt gauze as counter electrode. The potentials in this work have been converted to a reversible hydrogen electrode (RHE) reference electrode. Measurements were carried out in 0.1 M KOH saturated with O₂ (BOC). A thin-film catalyst layer was deposited on the glassy carbon electrode using a two-step drop-casting method with two different inks. An ink containing Vulcan XC-72 carbon and Na⁺-exchanged Nafion® (5 wt.%, Sigma-Aldrich) was deposited on the glassy carbon disk; followed by a deposition of an aqueous suspension of the oxide. The final loading in the catalyst layer for each electrode was controlled at 50 μg_{spinel} cm⁻² and 40 and μg_{Vulcan} cm⁻² (per geometric surface area of the electrode).

Consistent with previous reports, the as prepared Co-Fe spinels show high OER activity.^{8,9} As observed in Figure S6a and S6b, there is a good agreement between the results obtained for the film and powder samples: the activity increases with the amount of Co. This is evidenced by a 100 mV shift of the onset potential toward lower values as well as an increase of the current density when *x* increases from 0.6 to 2. All the catalysts show similar or better performance than Co₃O₄ and significantly outperform the activity of Fe₃O₄/Fe₂O₃. The Tafel analysis does not show significant differences in the reaction kinetics for the oxides with different composition, although FeCo₂O₄ showed the lowest Tafel slope (68 mV/dec) (Figure S6c).

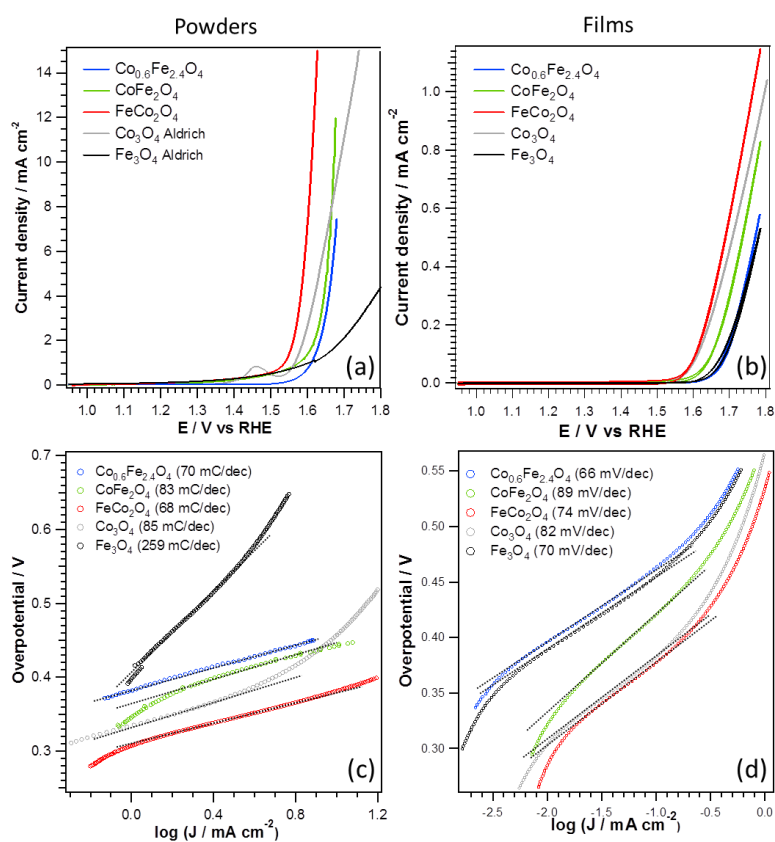


Figure S5. Electrochemical characterization. Linear sweep voltammetry (not IR corrected) (a,b) in O₂-saturated 0.1 M KOH and corresponding Tafel plots (c,d) for the Co-Fe spinel with different composition and the Co₃O₄ and Fe₃O₄ references in form of powders (a,c) and films (b,d).

In the case of the powders, a structure/activity relationship can be established by combining the structural and electrochemical characterization. In the literature, it has been previously reported that the catalytic performance of spinels is geometry-site-dependent;^{10,11,12} therefore, the structural characterization of these materials is crucial to rationalize their properties, in particular under working conditions. In order to investigate if the increase of the OER activity with the amount of Co is related to the geometric distribution of the Co atoms, the cation distribution was determined by EXAFS and Mössbauer Spectroscopy (Tables S1-S4). As seen in Table S1, the ratio between Co atoms in octahedral and tetrahedral sites ($\text{Co}_{\text{Oh}}/\text{Co}_{\text{Td}}$) decreases when the amount of Co increases, suggesting that the differences in OER activity should be related to Co atoms.

The results obtained from the *in situ* XAS measurements indicate that the Co(II) ions in tetrahedral sites are the most reactive ones and experience a chemical and structural evolution under the working conditions, leading to the formation of CoOOH which is considered the active catalytic phase. Actually, the activity of the Co-Fe spinel increases with the amount of Co(II)_{Td} species, confirming that the activity is related to the Co atoms and in particular, to Co(II) with tetrahedral coordination.

In situ chemical/structural characterization of the Co-Fe oxide thin films after the electrochemistry

Figure S7 shows the Co 2p XPS data for the Co-Fe-O/Pd(100) systems with different composition after the OER process. The Fe 2p region is not shown since no changes were observed for any of the materials: before and after the electrochemical measurement, Fe 2p lines characteristic of Fe(III) were obtained.

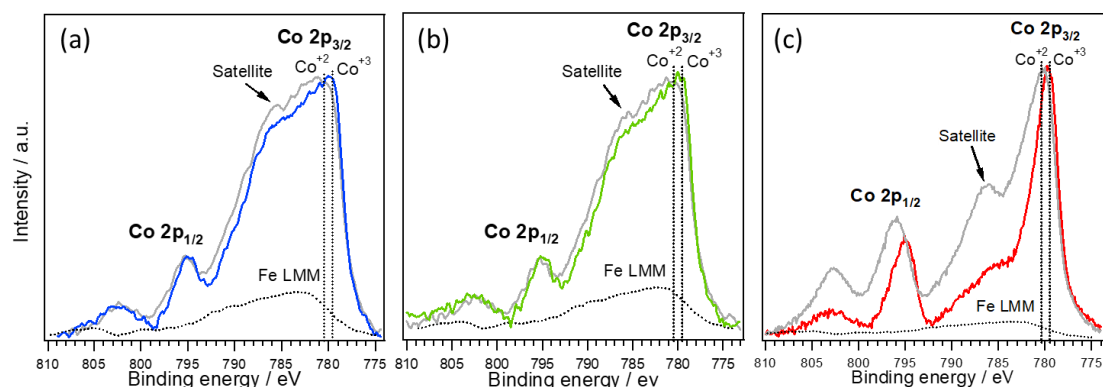


Figure S6. Co 2p photoemission spectra of the Co-Fe oxide films on Pd(100) substrate before (grey) and after (blue: $\text{Co}_{0.6}\text{Fe}_{2.4}\text{O}_4$; green: CoFe_2O_4 ; red: FeCo_2O_4) the electrochemical treatment. The spectra are shown after removal of the Shirley background.

The analysis of the Co 2p XPS data for the two ferrite films ($\text{Co}_{0.6}\text{Fe}_{2.4}\text{O}_4$ and CoFe_2O_4) shows a high stability of this phase. Only a slight oxidation of Co(II) to Co(III), evidenced by a slight shift in the BE of the Co 2p_{3/2} and Co 2p_{1/2} peaks to lower values and the decrease of the intensity of the satellite at 787 eV, is observed. On the other hand, significant changes in the FeCo_2O_4 film are deduced from XPS. The significant diminution of the spin orbit splitting

energy and the intensity of the satellite at 787 eV indicate a strong oxidation of the film leading to the formation of Co_3O_4 , as deduced from the Co 2p spectrum and the results for the CoO film showed in Figure 1.

Therefore, the *in situ* XPS/EC measurements suggest that the cobaltite phase is oxidized under OER conditions leading to the formation of Co_3O_4 and/or CoOOH . As a consequence of the Co oxidation, it is expected that Fe_2O_3 will also be formed, as seen in Figure 1. The ferrite phase, however, resulted to be very stable under OER conditions with only a slight oxidation of Co(II) to Co(III).

In situ XANES characterization of the Co-Fe oxide powders

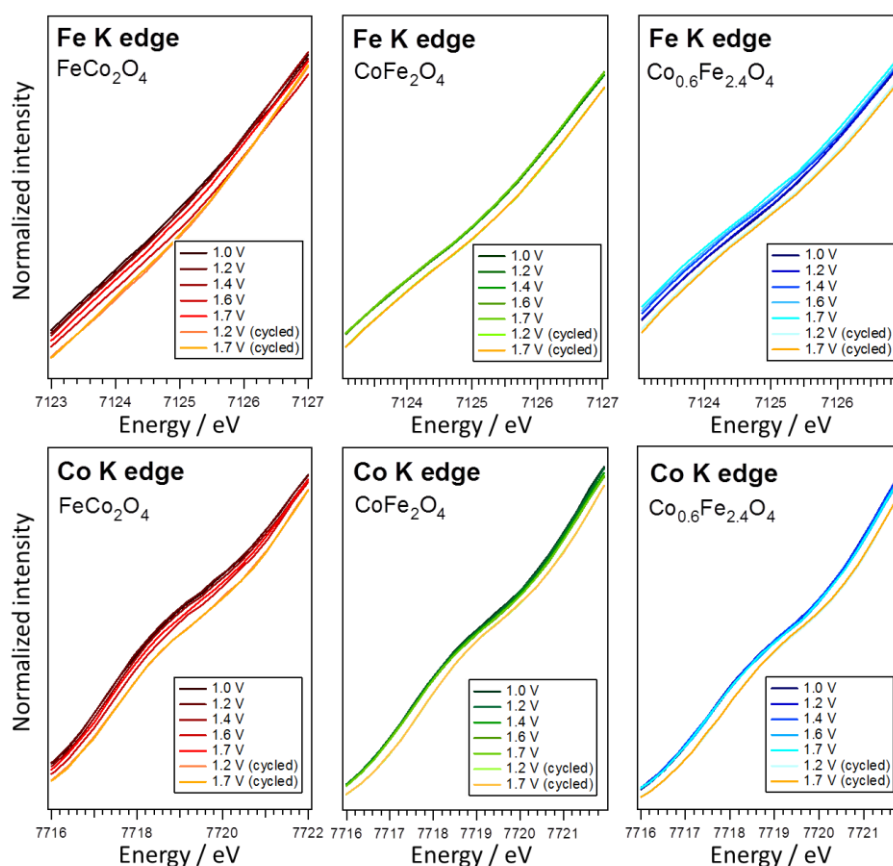


Figure S7. Detail of the shift of the Fe K (upper panels) and Co K (bottom panels) edges with the applied potential for the FeCo_2O_4 (red), CoFe_2O_4 (green) and $\text{Co}_{0.6}\text{Fe}_{2.4}\text{O}_4$ (blue) spinels.

TEM characterization of fresh and aged FeCo_2O_4 powder

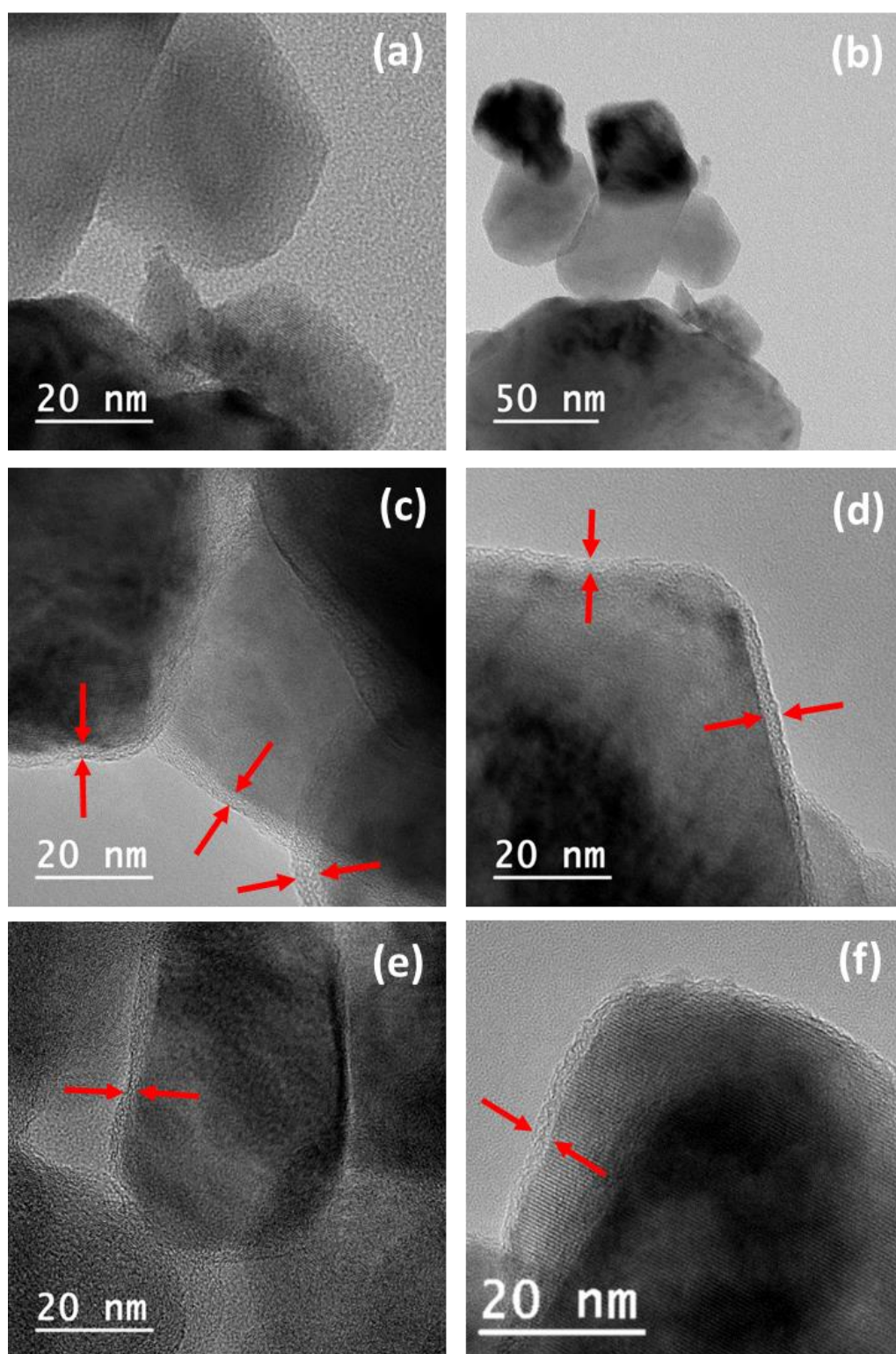


Figure S8. TEM images of the as-prepared (a,b) and aged (c-f) FeCo_2O_4 powder. The red arrows in (c-f) point out the amorphous layer.

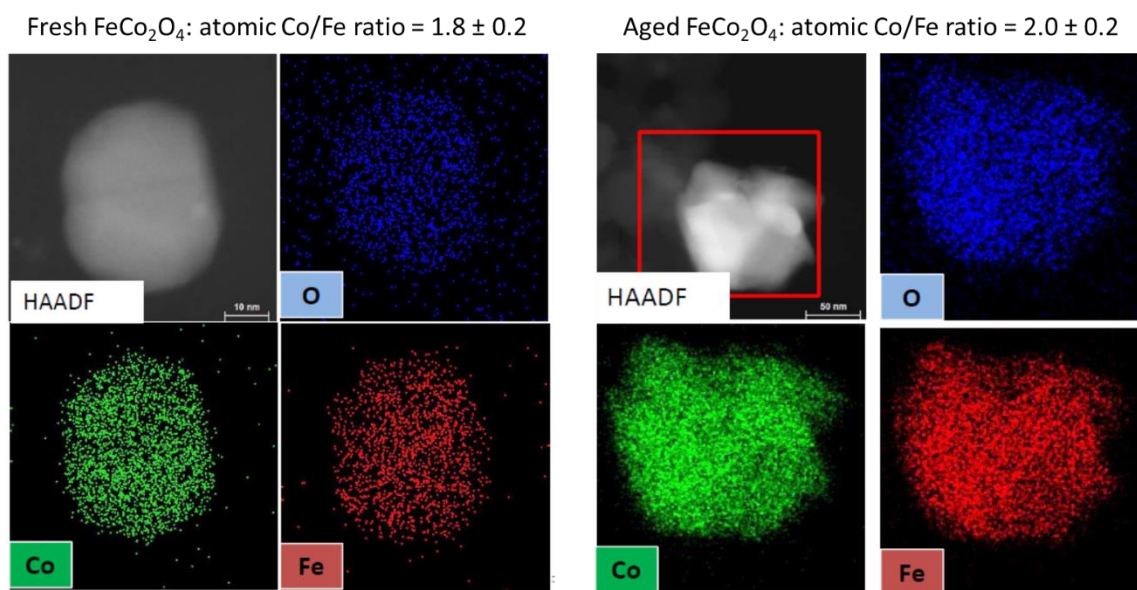


Figure S9. HAADF and EDS analysis of the fresh (left) and aged (right) FeCo₂O₄ sample.

References

- (1) M. C. Biesinger, B. P. Payne, A. P. Grosvenor, L. W.M. Lau, A. R. Gerson and R.St.C. Smart, *Appl. Surf. Sci.* 2011, **257**, 2717–2730.
- (2) O. Vozniuk, S. Agnoli, L. Artiglia, A. Vassoi, N. Tanchoux, F. Di Renzo, G. Granozzi and F. Cavani, *Green Chem.* 2016, **18**, 1038-1050.
- (3) B. Ravel and M. Newville, *J. Synchrotron Rad.*, 2005, **12**, 537.
- (4) M. Newville, *J. Synchrotron Rad.*, 2001, **8**, 96.
- (5) C. Li, X. Han, F. Cheng, Y. Hu, C. Chen and J. Chen. *Natur. Commun.* 2015, **6**, 7345.
- (6) F. Jiao and H. Frei. *Chem. Commun.*, 2010, **46**, 2920–2922.
- (7) M. Belli, A. Scafati, A. Bianconi, S. Mobilio, L. Palladino, A. Reale, E. Burattini. *Solid State Commun.*, 1980, **35**, 355-361.
- (8) X.-F. Lu, L.-F. Gu, J.-W. Wang, J.-X. Wu, P.-Q. Liao and G.-R. Li, *Adv. Mater.* 2017, **29**, 1604437.
- (9) W. Bian, Z. Yang, P. Strasser and R. Yang, *J. Power Sources* 2014, **250**, 196-203.
- (10) H.-Y. Wang, S.-F. Hung, H.-Y. Chen, T.-S. Chan, H. M. Chen, B. Liu. *J. Am. Chem. Soc.* 2016, **138**, 36-39.
- (11) C. Schwanke, H. S. Stein, L. Xi, K. Sliozberg, W. Schuhmann, A. Ludwig and K. M. Lange, *Sci Rep.* 2017, **7**, 44192.
- (12) X. Wang, Y. Liu, T. Zhang, Y. Luo, Z. Lan, K. Zhang, J. Zuo, L. Jiang and R. Wang, *ACS Catal.* 2017, **7**, 1626–1636.